Wireless Sensor for Continuous Real-Time Oil Spill Thickness and Location Measurement

Hovig Denkilkian, *Student Member, IEEE*, Agop Koulakezian, *Student Member, IEEE*, Rostom Ohannessian, *Student Member, IEEE*, Milad S. Chalfoun, Mohamad Khaled W. Joujou, Ali Chehab, *Senior Member, IEEE*, and Imad H. Elhajj, *Senior Member, IEEE*

***Abstract*—Marine pollution by oil spills is a devastating environmental hazard, requiring a low-cost efficient system for continuous and real-time thickness measurement and localization of oil. Knowing that none of the previous detection methods has managed to fully meet these requirements, it is necessary to devise a new technique for guiding and speeding up the clean-up process of oil spills. This paper presents a sensor device that is capable of sensing, processing, and transmitting information about an oil spill (location and thickness). This paper discusses two new methodologies of detection based on the difference in the absorbance spectral signatures and electric conductivity properties of oil and water. This paper also discusses the mechanical design of the device, the hardware implementation of its components, and the integration and evaluation of the whole system. The experimental results confirm the effectiveness of the proposed method under different lighting, salinity, temperature, and sea conditions.**

***Index Terms*—Conductivity measurement, marine equipment, oil localization, oil spills, thickness measurement.**

I. Introduction

OIL SPILLS are catastrophic environmental events, which are highlighted by the destructive accidents of Prestige, Erika, and Exxon Valdez. They are mainly caused by ship spills, pipeline leaks, and offshore drilling operations [1]. Given that oil slicks quickly spread and cannot be extracted once they become very thin, usually, only 20% of the total quantity of the oil is recovered from a spill [1]. Therefore, proper treatment of oil spills necessitates a rapid and well-resourced response. Knowing that a real clean up is not possible in most cases, containing the oil spill through booms reduces the extent of the damage. This step is followed by recovering the oil into a receiving tank using skimmers. Studies have shown that knowing the oil slick thickness at different locations minutes after an oil spill occurs cuts down the clean-up costs, because it helps guide the clean-up operation by indicating the real-time path for the most efficient treatment, starting with the thickest location of the oil slick. This is because response personnel can more effectively plan countermeasures (different countermeasures are adopted for different oil thicknesses ranging from 0 to 600 mm [12]) while attempting to limit the effects of the pollution [2]. Moreover, direct-contact measurement of the thickness, compared with existing techniques, is more resistant to weather conditions and effective with different types of oils. While remote sensing, mainly using synthetic aperture radar (SAR) and laser fluorosensor techniques, is the most common form of oil spill tracking, it suffers from many drawbacks, such as delayed response, high cost, and dependence on weather, lighting, temperature, and sea conditions [3].

To solve the problem at hand, a low-cost wireless sensor node was designed and implemented, to be placed on board oil tankers and offshore drills. Right after or as an oil spill occurs, a number of such devices can be thrown into the spill, adhering to the oil slick above the water surface. As the oil slick spreads, the devices will move away from each other while floating around with the slick, sensing, processing, and transmitting information about the oil spill. Since the maximum wireless communication range of each node is 1 km, there should be at least one sensor node in every square kilometer of area. Using a large number of these devices will produce a map of the current state of the oil spill, including its thickness level at different locations in a short amount of time, guiding a fast and efficient treatment of the spill. Furthermore, the device is designed and tested to provide accurate results under various atmospheric and oceanic conditions and in different geographic regions.

II. Related Work

Infrared thermal sensing is based on the fact that oil films emit heat slower than the surrounding water during daytime. However, the process is reversed during nighttime, making it vulnerable to lighting conditions. As mentioned in [4], the Advanced Spaceborne Thermal Emission and Reflection Radiometer, which is used on NASA's Earth Observation System, relies on the thermal inertia and temperature differences between oil and water in identifying oil spill locations. Since oil weathering (change in the chemical composition of oil) may change, the difference in these characteristics over time and the

Manuscript received June 26, 2008; revised December 2, 2008. Current version published November 11, 2009. This work was supported by the Department of Electrical and Computer Engineering, American University of Beirut. The Associate Editor coordinating the review process for this paper was Dr. Robert Gao.

H. Denkilkian, M. K. W. Joujou, A. Chehab, and I. H. Elhajj are with the Department of Electrical and Computer Engineering, American University of Beirut, Beirut 1107 2020, Lebanon.

A. Koulakezian and R. Ohannessian were with the Department of Electrical and Computer Engineering, American University of Beirut, Beirut 1107 2020, Lebanon. They are now with the Department of Electrical and Computer Engineering, University of Toronto, Toronto, ON M5S 3G4, Canada.

M. S. Chalfoun was with the Department of Electrical and Computer Engineering, American University of Beirut, Beirut 1107 2020, Lebanon. He is now with Polytronics, Jounieh, Lebanon.

Color versions of one or more of the figures in this paper are available online at http://ieeexplore.ieee.org.

Digital Object Identifier 10.1109/TIM.2009.2021641

warm-to-cool transition of oil are not sharply defined; as a result, the accuracy of the performed measurements is limited [5].

Radar sensing, which is another remote sensing technique for detecting oil spills, is based on the backscatter of the microwave signal transmitted by the radar, making it strongly dependent on wind and sea conditions. In [6], the ScanEx R&D Center has found a complete solution for the fast acquisition, processing, and monitoring problem of oil spills using SAR imagery. The captured SAR images are prone to error due to the short waves that are usually present on the seawater surface and the fact that oil films affect the viscosity of the seawater [3]. More importantly, SARs do not provide a thickness estimate for the oil spill.

Certain ultrasonic characteristics of oil can also be used to identify the oil in seawater and estimate its thickness in two ways: The first is based on applying an ultrasonic pulse to an oil film and measuring the amplitude or phase angle of the reflected signal, knowing that the reflection coefficient of oil depends on its thickness and acoustic properties [7]. The second is based on measuring the time delay of an ultrasonic wave between the air–oil and oil–water boundaries. This approach was adopted in the design of the Laser Ultrasonic Remote Sensing of Oil Thickness system [8], which was developed by the Industrial Materials Institute, National Council Research Canada. Ocean currents, which cause changes in the phase of the reflected signal, lead to inaccurate results, limiting the usage of this technique.

Laser fluorosensors, such as the Scanning Laser Environmental Airborne Fluorosensor [9], are based on the fact that different types of oil fluoresce at different wavelengths and have different deterministic spectral signatures. The captured fluorescence spectra are investigated through a principle component analysis to determine the presence of oil. However, these devices have some drawbacks, such as their large size, heavy weight, and high cost [2].

Hyperspectral imaging can be used to build a library of spectral signatures for different types of oil, to be used for oil detection [10]. Another multispectral technique determines the oil thickness by computing ratios between specific wavelengths in the absorbance spectrum of oil. According to [11], spectral ratios, which are less sensitive to light fluctuations than radiance, vary as a function of the properties of seawater and the spectral quality of incident light. Thus, assigning an absolute thickness to a specific spectral ratio is not accurate.

In conclusion, most of the current detection methods addressing the stated problem rely on remote sensing (thus requiring the use of a dedicated aircraft) and are strongly affected by the lighting, temperature, and weather conditions, in addition to being associated with high cost.

There are a few direct-contact techniques for tracking oil spills that depend on capacitance and electric conductivity. The former, which was mentioned in [12], is based on the difference in relative permittivity between oil and water. However, this technique requires on-site calibration and is dependent on the type of oil. Moreover, the wetting of electrodes in this technique is challenging due to the sensitivity of capacitance. A method using electric conductivity uses a motor to immerse two electrodes in the oil above the water, until they reach the oil–water boundary, and calculates the oil thickness according to the number of revolutions [13]. However, this method is dependent on the stability of the device above the water surface, which cannot be achieved due to oceanic waves and wind speeds. In addition, it includes movable parts, which could malfunction when immersed in dense oil.

III. System Design and Implementation

A. Thickness Measurement Sensors

Two independent techniques were designed and implemented to determine the thickness of the oil, i.e., the use of a light sensor array and a conductivity array.

1) Light Sensor Array: This is an active optical color sensor based on the concept of variation of intensity and the properties of light propagating in a certain medium. The amount of received power of light on the receiving surface per unit area, on the other end of the propagating medium, is referred to as *illuminance*. Since blue light exhibits very low absorption in water [14] and high absorption in oil [15], [16], the decision was to use blue LEDs as the source of light. Since the required low-cost receiver of blue light should only detect wavelengths in a narrow range between 440 and 490 nm, the most suitable receiver was found to be the light-dependent resistor (LDR), whose resistance inversely varies (in an exponential fashion) with the change in intensity of the light received on its surface. Therefore, a longitudinal array of LED–LDR pairs was used, as shown in Fig. 3, through which the change in the resistances of the LDRs can be measured to detect the oil level, based on the fact that, when the blue light passes through the water, the LDR resistance is low and, when it passes through the oil, its resistance is high.

Although this detection method requires the measurement of resistances, the actual measurements in the implemented system design are voltages. Since the value of an LDR can vary on the order of hundreds, it would be impossible to physically implement a current source for changing the LDR resistance to voltage that can be entered to the microcontroller. Therefore, to get the LDRs' resistance values, voltage V_L on LDR R_L was measured using a voltage divider configuration fed with a known voltage ($V_{dd} = 5$ V), where each of the LDRs is placed in series with another resistor R_C of known value, as shown in (1). Thus, the resistance of the LDR is calculated using (2)

$$V_L = \frac{V_{dd} \times R_L}{R_C + R_L} \tag{1}$$

$$R_L = \frac{V_L}{V_{dd} - V_L} R_C. \tag{2}$$

In order for V_L to linearly vary with R_L in (1), R_C should have a very large value. However, this would lead to a very small value of V_L, which would be difficult to read using the A/D input of the microcontroller. Conversely, making the value of R_C very small would make V_L independent of R_L and, thus, irrelevant to our analysis. Therefore, we have chosen the value of R_C to be 1 kΩ, which is in between our range of possible LDR values under different lighting conditions. This will enable us to retrieve the LDR resistance values through simple calculations in the microcontroller, using (2).

2) Conductivity Array: This is a passive sensor based on the difference in electric conductivity properties of different aqueous solutions. The conductivity of water is dependent on the concentration of dissolved salts and other chemicals that ionize in it. Since sea water possesses high electric conductivity and oil possesses low electric conductivity, the current passing through sea water is high, and the current passing through oil is low. Therefore, a longitudinal array of conductive metal pairs (similar to that of the longitudinal array of LED–LDR pairs and composing of two plates) is used. One plate is fully covered with conductive material and connected to ground, and another plate is covered with equidistant strips of the same conductive material, as shown in the bottom part of Fig. 3, which are fed by a constant voltage and separated by strips of nonconductive material having the same thickness. Each strip of conductive metal, along with the fully conducting plate, makes up a conductive metal pair, which is separated by oil or water. By measuring the intensity of the current passing through each conductive pair, we can detect the presence of oil of a certain depth. As in the case of the light sensor array, voltages are being measured. Therefore, each conductive pair is connected to resistor R_D to transform the measured current to voltage. R_D should have a small resistance value in order not to attain high voltages at the A/D input of the microcontroller.

Since the aqueous solution between each conductive pair does not act like a perfect switch, where it is on in the case of water and off in the case of oil, it is better to measure conductivity using resistance, where the aqueous solution acts like a resistor, which is high in the case of oil and low in the case of water. Therefore, measuring the voltage on R_D is almost equivalent to the voltage divider configuration used for the light sensor array. However, no initial calculation (to convert voltage into current intensity) is needed since the measured voltage is linear to the current intensity, which is required for the analysis. To prevent ground looping, which can be caused by the existence of a large number of resistors in series with each metal strip, the resistors are connected to a multiplexer, through which only one of the resistors is connected to ground at one time.

B. Hardware Implementation

1) Hardware Components: The block diagram of the device is shown in Fig. 1. In addition to the light sensor and conductivity arrays, it includes a GPS module, which is used to locate the geographical position of the sensor in the oil spill and a radio transceiver, which is used to transmit information about the oil spill, including the thickness and position of the oil. It also includes a PIC microcontroller, which is used to process the measurements collected by the light sensor and conductivity arrays to determine the thickness of the oil, based on the devised detection algorithms (which is discussed later).

For the GPS module, the EM-411, which is manufactured by GlobalSat, was chosen mainly because of its relatively low cost, number of channels, short synchronization time, and built-in antenna features. For the transceiver, the EVAL-315-LT evaluation board was selected because of its low power consumption, large transmission range, and serial interface. For the microcontroller, the ET-PIC Stamp evaluation kit is used

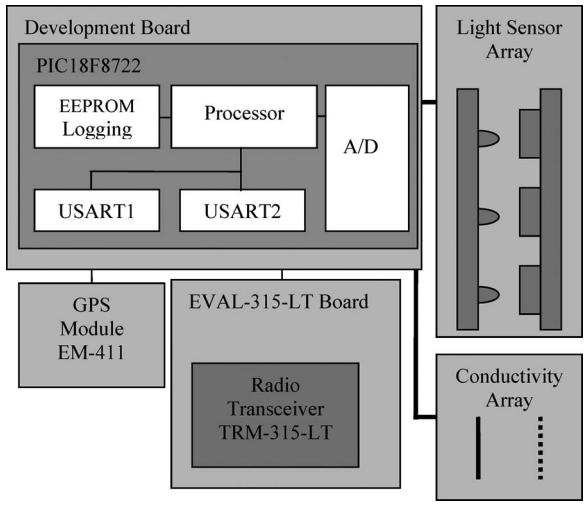

Fig. 1. Block diagram of the hardware system.

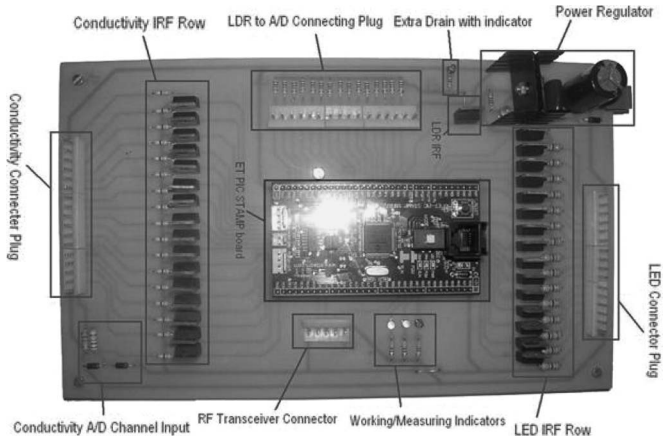

Fig. 2. Processing board.

because of its compact form, the PIC18F8722 microcontroller it includes, its two serial port interfaces, and its 16-channel 10-bit A/D converter.

2) Component Integration: The processing board (Fig. 2) acquires data from the two arrays of sensors. In conjunction to reading these data, it also needs to control some devices, such as the LED array, transceiver, and GPS module. The adopted design requires the control and measurement of 15 LED–LDR pairs, with an additional A/D channel reserved to the conductivity array. The conductivity array needs to control the current flowing through each conductor one at a time to capture precise data. The PIC controls 15 transistors that are used to turn the conductivity strips needed to measure the corresponding voltage levels on and off. As for measuring, the conductivity plate is connected to the ground through a 4.7-Ω resistance and to the A/D input through a protective 1-kΩ resistance. Since the conductivity array is directly in the water and, thus, may be prone to voltage changes, clamping diodes are used as a protective measure, so that the input voltage does not rise over 5 V or fall below 0 V.

The GPS module that was used is the EM-406 from GlobalSat, which incorporates a SirfStar III chip. The module size is 3×3 cm and has a built-in antenna. It supports different protocols of communication, out of which we decided to work

with the world standard NMEA-0183 ASCII protocol. The GPS module has a continuous update system that constantly sends different commands to the listener, with information about its position and satellite location. It requires a 5-V supply, and communication is through the full-duplex RX/TX ports. The 1 pulse per second is a signal used for clock synchronization since the GPS also offers the current Greenwich Mean Time to the host, which is needed for synchronous real-time measurements.

The TRM-433-LT transceiver module transmits modulated data signals in the 433-MHz band to establish a working wireless communication link between a PC and a sensor. The module supports on–off keying and has two-wire communication using a T/R select and a data pin. On both sides of the communication link, different modules were implemented to interface the PC and PIC with the transceiver boards. The communication is accomplished through a half-duplex channel. The MODBUSS communication protocol was implemented to use the predefined commands of control and the built-in error detection facility (cyclic redundancy check). The mentioned setup allows the transceiver to accept data from the microcontroller through the ET-PIC Stamp Module and send timely information about the location and thickness of oil satisfying the real-time requirements of oil sensing. In later design iteration, the wireless communication module will be selected according to the stringent criteria on power consumption, baud rate, and dimensions.

The design comprised as few parts as possible for simplicity and rapid assembly, so that the functionality requirements of the sensor are delivered. For future implementations, components that are easily available in the market and minimize the overall cost of the spill sensor to make the device more attractive should be used.

In addition, the surface-mount device technology should be employed to minimize the total space occupied by the components.

C. Oil Adhesion

Since the device will be thrown in the open oceans, the molecular attraction exerted between the surface of the device and the spilled oil is not guaranteed, due to the presence of different biological microorganisms. Hence, the direct-contact sensing method necessitates the choice of a material that is much more adhesive to oil than to water. Different materials solve the problem of adhesion on a microscopic level due to their high surface energy, which allows easier spreading of the oil on a given surface. As an example, oleophilic elastomers (elastic polymers), such as neoprene and hypalon, were widely used in the manufacturing of oil-skimming products [17]. However, other alternatives that deal with the problem of surface contact between rough surfaces and oil at the macroscopic level can be considered and are more attractive, because a complete packaged device is constructed in this work. Based on the difficult experience in the cleanup of birds covered in oil, one of the alternatives in accomplishing strong adhesion to oil was actually to cover the top part of the sensor with featherlike material. However, upon testing the prototype with heavy fuel oil, it was found that heavy fuel oil instantly adheres to many materials. The buoy used to float the sensor, which is made of organic polymers, sufficiently adhered to oil to maintain contact with the oil while floating.

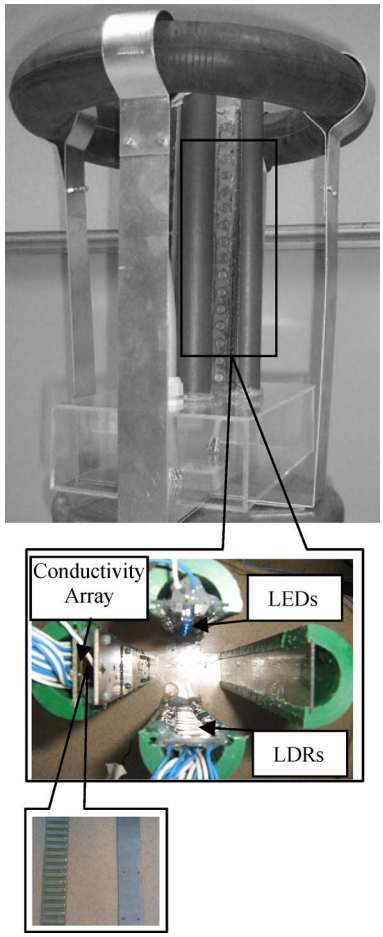

Fig. 3. Mechanical design.

D. Mechanical Design

The study of the mechanical design of the sensor is necessary for assessing the stability and buoyancy of the device in a real-life marine environment. Moreover, this enables monitoring of the effect of wind speeds and oceanic waves on the accuracy of the thickness measurement generated by the device. The proposed design (Fig. 3) relies on a floating inflatable tube that is connected to a 20×30 cm box, which is made of plexiglass, has a height of 8 cm, and contains each of the three electrical boards that were designed for the purpose of data processing, communication, and GPS data acquisition. This connection is made through four strips of aluminum (with a thickness of 1.5 mm) that are wrapped around the tire tube in diametrically opposite positions using screws. These strips are connected to each other at the center of the box from the bottom using a screw. As for the sensing unit, the four columns of sensors form a rigid body and are connected to the top surface of the component box. The implemented design ensures the buoyancy and stability of the device through the use of a floater with the necessary surface area and the addition of some weight at the bottom of the device.

IV. Thickness Detection Algorithms

A. Light Sensor Array

Algorithm 1 describes the analysis of the measured data using the light sensor array to determine the thickness of the oil. It first takes the averages of k voltage measurements. Then, it calculates the LDR values from the corresponding voltage measurements using (2). Since a small error in voltage measurement may produce a large change in the resistance value ($V_L = 4.98$ V and $R_L = 249$ kΩ, while $V_L = 4.99$ V and $R_L = 499$ kΩ), the algorithm replaces all R_L values larger than $R_M = 1$ MΩ by 1 MΩ, which is 1000 times larger than R_C and was the maximum resistor value obtained through direct experimental measurement. The logarithm of each resistance is taken into account for the exponential response of LDRs with the change in intensity. This is followed by determining the ratio of the resistances between the cases when the blue LEDs are turned off (R_D) and when they are turned on (R_B). This will remove the offset in the resistance values, which is caused by changing lighting conditions, and will eliminate the need for on-site calibration of the LDRs before detection. Every one of these ratios $R(i)$ is then divided by its previous value, and the changes between these ratios are enlarged using an exponential. The maximum of these ratios corresponds to the pair of consecutive LDRs where the oil–water boundary exists. Therefore, the thickness of the oil is determined with a quantization error equal to $D/2$, where D is the distance between two consecutive LDRs.

B. Conductivity Array

Algorithm 2 describes the analysis of the measured data using the conductivity array to determine the thickness of the oil. It first takes the averages of k voltage measurements on R_D. Since conductivity measurements change with the water salinity (see experimental results), every one of these voltages $V(i)$ is then divided by its previous value, and the maximum of these ratios corresponds to the pair of consecutive conductive pairs where the oil–water boundary exists. To detect the "no-oil" case, the algorithm checks if the maximum ratio is larger than R_T, which is usually set to 5. Therefore, the thickness of the oil is determined with a quantization error of $D/2$, where D is the distance between two consecutive conductive strips.

Algorithm 1: Thickness Using the Light Sensor Array

Data: matrix V_B and matrix V_D of voltages with the blue light on and off, respectively;
V_{dd}, which is the voltage for the voltage divider;
R_C, which is the resistance in series with the LDR;
D, which is the distance between two consecutive LDRs;
R_M, which is the maximum possible value for a resistor.

Result: thickness of the oil (same unit as d).

Initialization: Set m to the number of LDRs used.
Set k to the number of times that each measurement is repeated.
Set max to 0 and $index$ to -1.

Step 1: Take the averages of k voltage measurements with the blue light on and off.

for $i = 1, \ldots, m$ **do**

$$L_B(i) = \text{average}\,(V_B(i), k)$$
$$L_D(i) = \text{average}\,(V_D(i), k)$$

end

for $i = 1, \ldots, m$ **do**

Step 2: Calculate the LDR values from the corresponding voltage measurements using (2), i.e.,

$$R_B(i) = \frac{L_B(i)}{V_{dd} - L_B(i)} \times R_C$$
$$R_D(i) = \frac{L_D(i)}{V_{dd} - L_D(i)} \times R_C.$$

Step 3: Replace all R_L values that are larger than $R_M = 1$ MΩ by 1 MΩ. Take the logarithm of each resistance.

if $R_B(i) > R_M$ **then**
$R_B(i) = \log(100 \times R_M, 10)$
else
$R_B(i) = \log(100 \times R_B(i), 10)$
if $R_D(i) > R_M$ **then**
$R_D(i) = \log(100 \times R_M, 10)$
else
$R_D(i) = \log(100 \times R_D(i), 10)$

Step 4: Find the ratios of the resistances between the cases when the blue LEDs are turned off (R_D) and when they are turned on (R_B), i.e.,

$$R(i) = \frac{R_D(i)}{R_B(i)}.$$

end

Step 5: Divide each ratio $R(i)$ by its previous value, and enlarge the changes between them using an exponential. Find the maximum of these ratios, and return the index of this maximum ratio multiplied by the resolution.

for $i = 1, \ldots, m-1$ **do**
Ratio$(i) = 10^{(R(i+1)/R(i))}$
if Ratio$(i) > \max$ **then**
$index = i$
$\max =$ Ratio(i)
end
return $(index) \times D$

Algorithm 2: Thickness Using the Conductivity Array

Data: matrix V_R of voltages across the resistor in series with each conducting pair;
R_T, which is the minimum threshold ratio;
D, which is the distance between two consecutive conducting strips.

Result: thickness of the oil (same unit as d).

Initialization: Set m to the number of conducting pairs.
Set k to the number of times that each measurement is repeated.
Set $index$ to -1 and max to 0.

Step 1: Take the averages of k voltage measurements.
for $i = 1, \ldots, m$ **do**
  $V(i) = \text{average}(V_R(i), k)$
end for
Step 2: Divide each voltage $V(i)$ by its previous value, obtaining the following:
Ratio(i)
for $i = 1, \ldots, m-1$ **do**
  Ratio$(i) = V(i+1)/V(i)$
end for
Step 3: Find the maximum of these ratios, and return the index of this maximum ratio multiplied by the resolution.
for $i = 1, \ldots, m-1$ **do**
  if Ratio$(i) > \max$ **then**
    $index = i$
    $\max = \text{Ratio}(i)$
  end if
end for
if $\max < R_T$ **then**
  $index = 0$
end if
return $(index) \times D$

V. Experimental Setup and Results

A. Experimental Setup

The designed prototype submerged in oil and sea water is shown in Fig. 4. The experiments were carried out in an experimental tank containing water and oil under different lighting conditions (light and dark), water types (fresh and salt), and oil thicknesses, with and without waves. The 16 LDR–LED pairs used are aligned with each other, having their centers exactly $D = 2$ cm apart from each other. The LDRs have a diameter of 10 mm, whereas the LEDs have a diameter of 5 mm. The distance between an LDR and its corresponding LED is exactly 7.6 cm. The LEDs are supplied by 4 V (dc), because the light source should generate enough radiant energy that can pass through the oil and reach the receiver with adequate intensity, so that any variation in transparency/opacity due to oil is detectable. The center of the first LDR is at the surface of the water under flat-sea conditions. Unlike the surface of the ocean, the experimental tank being used has limited surface area. Thus, whenever the thickness of oil was, e.g., 2 cm, and the first LDR from above was covered by oil, light from the outside or other LEDs would still pass beneath this oil surface, with an angle reaching the LDRs below it. As the thickness of the oil increases, the possible values of this angle decrease, making it harder for exterior light or light from other LEDs to cause interference to the LEDs below. This concept is referred to as the shadowing effect. The experimental results in [18] showed that, for the light sensor array, the results improved with the thickness of the oil, and this was visible through higher peaks and percentage difference values from the closest (second) obtained ratios. This was caused by the shadowing effect of the oil, which decreased the interference from the environment and between the LEDs. Therefore, in the following experiments, the LEDs were successively turned on in groups of four (with LEDs 1, 5, 9, and 13 simultaneously turned on and then LEDs $2, 6, 10, 14, \ldots$) to decrease the interference between them.

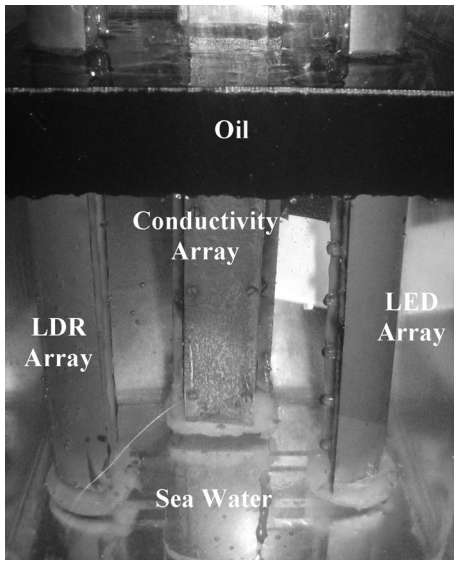

Fig. 4. System prototype.

Each of the 32 conductive pairs used has a thickness of 0.5 cm, and the pairs are separated by a 0.5-cm-thick nonconductive strip. The stripped plate is separated from the fully conducting plate by a distance of 6.5 mm. While a large distance would produce a low current, which is difficult to accurately measure, a smaller distance could make the oil get stuck between the plates, producing inaccurate results. Resistance R_D, the voltage of which was measured in the conductance array, had a value of 4.7 Ω. Both the LDRs and the conductive pairs are numbered in increasing order from top to bottom. The center of the first strip is 0.5 cm below the surface of the water. The conductive metal used was copper, which slowly underwent some electrolysis; thus, it would be worn out after a few hours of continuous use. The electrolysis incurred by the conductivity array, as shown by the experimental results in [18], was reduced by tinning the copper material of the array. This was further reduced through a technique called "cleaning cycle using reverse voltage." Whenever a conductive strip is fed with a 5-V dc voltage, some cations electrolyze from it and stick on the surface of the fully conductive plate, lowering the voltage values of further measurements. Therefore, a cleaning cycle was used for the following experiments before each measurement, where the 5-V dc voltage was fed to the fully conductive plate, and the specific conductive strip was grounded. Moreover, successively taking 30 measurements for each conductive pair and repeating this process every 10 min will increase the life of the conductivity plates to two or three days, which is the required life span of the sensor device.

B. Light Versus Dark Experiments

These experiments were conducted using only the light sensor array (since the conductivity array is not affected by varying lighting conditions) under light and dark environments and with different thicknesses of oil. The thickness levels examined are 2 cm apart from each other, because the resolution of the device

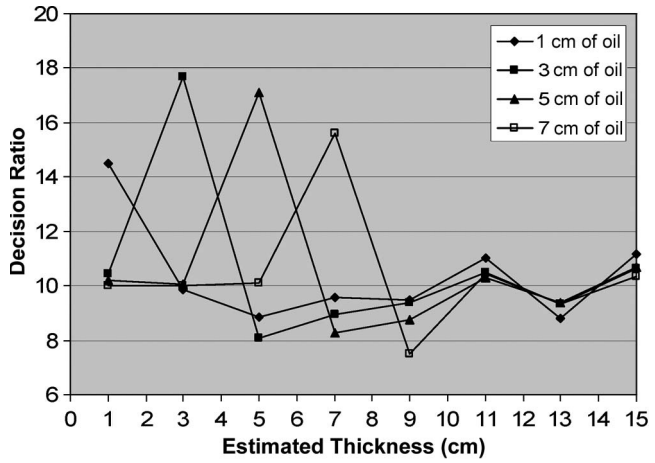

Fig. 5. Thickness measurement using LDRs (light environment).

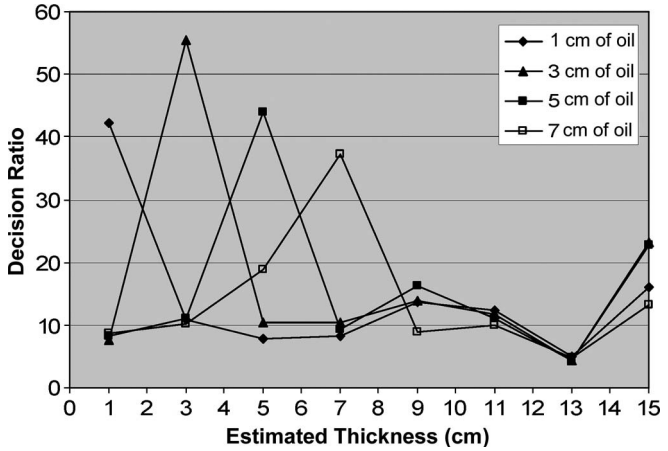

Fig. 6. Thickness measurement using LDRs (dark environment).

is equivalent to the distance between the centers of two consecutive LDRs in the array. The experiment was carried out using fresh water at room temperature and with no waves. Figs. 5 and 6 show the results after using Algorithm 1. These graphs show the ratios explained in Algorithm 1, where the maximum peaks of these ratios represent the estimated thickness, which can be read on the x-axis of the graph. Each of the three curves, in both figures, has its peak at its corresponding thickness read on the x-axis. Therefore, the conducted experiments have not produced any errors.

Table I shows the percentage difference between the peak of each curve and the closest (second) obtained ratio. The table shows that, even if the highest ratio, below the maximum ratio, increases, due to experimental errors, by the given percentage in the table, the results of the algorithm would still have given correct estimates of the thickness. From both of these graphs, one can see that the results are similar under both conditions.

TABLE I
PERCENTAGE DIFFERENCE BETWEEN THE PEAK OF EACH CURVE AND THE CLOSEST OBTAINED RATIO

Oil Thickness Levels	Light	Dark
1 cm	29.9%	162.7%
3 cm	66.4%	139.0%
5 cm	60.6%	93.2%
7 cm	49.3%	183.7%

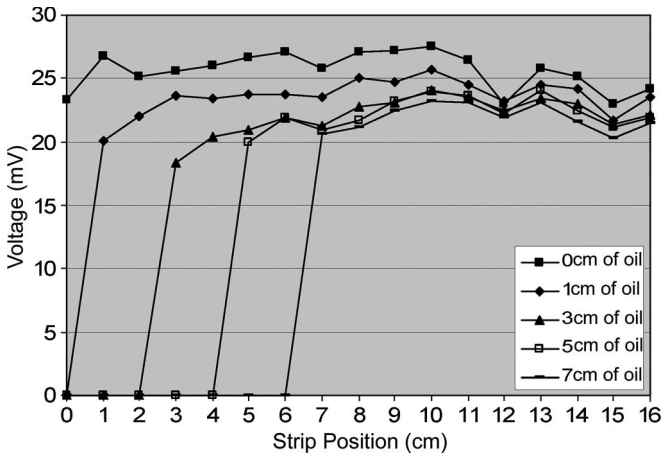

Fig. 7. Conductivity array results (fresh water).

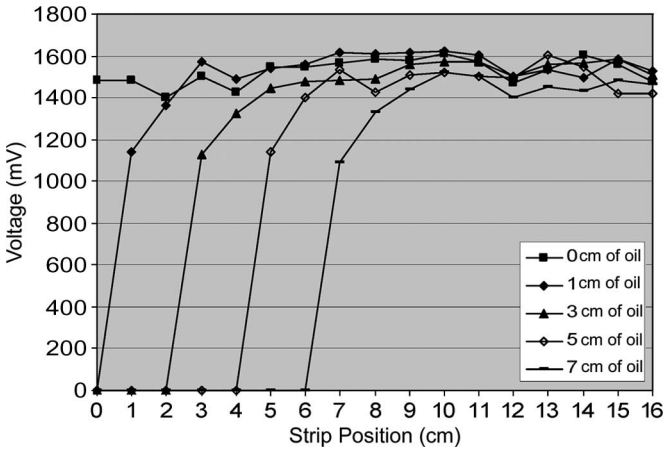

Fig. 8. Conductivity array results (salt water).

C. Fresh Water Versus Salt Water Experiments

These experiments were conducted using only the conductivity array (since the light sensor array is not affected by varying water salinity) with both fresh and salt water, and different thicknesses of oil. The experiment was carried out under light conditions at room temperature and with no waves. The highest ratio in each set of measurement (according to Algorithm 2), given that it is higher than a threshold (about 5), represents the estimated thickness, which can be read in the shaded cell of the table associated with each graph.

Figs. 7 and 8 show the results of the experiments conducted with the two types of water. Their corresponding tables are Tables II and III, respectively. These results show no errors. From both of these graphs, it is seen that the results are similar under both conditions.

D. Temperature Change Experiments

These experiments were conducted with both of the arrays with 3 cm of oil. The experiment was carried out using salt water under light conditions and with no waves. Figs. 9 and 10, along with Tables IV and V, show the results, showing no

TABLE II
CONDUCTIVITY ALGORITHM RESULTS (FRESH WATER)

Estimated Thickness	Actual Thickness				
	0 cm	1 cm	3 cm	5 cm	7 cm
1 cm	1.1	6010.0	1.3	0.0	0.7
2 cm	0.9	1.1	1.8	0.0	2.0
3 cm	1.0	1.1	612.4	0.0	1.3
4 cm	1.0	1.0	1.1	1.1	0.8
5 cm	1.0	1.0	1.0	666.3	2.8
6 cm	1.0	1.0	1.0	1.1	1.1
7 cm	1.0	1.0	1.0	1.0	515.7
8 cm	1.0	1.1	1.1	1.0	1.0

TABLE III
CONDUCTIVITY ALGORITHM RESULTS (SALT WATER)

Estimated Thickness	Actual Thickness				
	0 cm	1 cm	3 cm	5 cm	7 cm
1 cm	0.7	114166	1.0	1.5	1.5
2 cm	1.0	1.2	0.8	1.0	1.0
3 cm	0.9	1.2	84750	0.7	0.7
4 cm	1.1	0.9	1.2	1.5	2.0
5 cm	1.0	1.0	1.1	57033	0.3
6 cm	1.1	1.0	1.0	1.2	3.0
7 cm	1.0	1.0	1.0	1.1	108866
8 cm	1.0	1.0	1.0	0.9	1.2

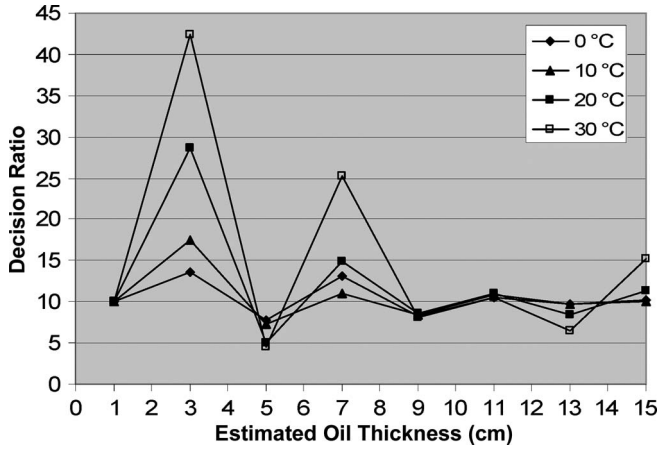

Fig. 9. Thickness measurement using LDRs (changing temperatures).

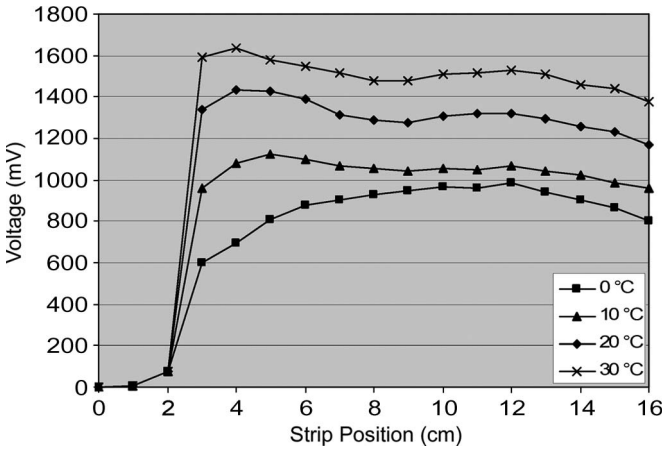

Fig. 10. Conductivity array results (changing temperature).

errors. From these graphs, it could be concluded that both of the arrays work better at high temperatures since the decision ratio and voltage difference are increasing with temperature.

TABLE IV
PERCENTAGE DIFFERENCE BETWEEN THE PEAK OF EACH CURVE AND THE CLOSEST OBTAINED RATIO (CHANGING TEMPERATURE)

0 °C	4.3%
10 °C	60.1%
20 °C	92.2%
30 °C	67.6%

TABLE V
CONDUCTIVITY ALGORITHM RESULTS (CHANGING TEMPERATURE)

Estimated Thickness	Temperature (Actual Thickness = 3 cm)			
	0 °C	10 °C	20 °C	30 °C
1 cm	2.3	3.4	3.5	2.4
2 cm	8.1	12.2	11.4	15.6
3 cm	13.3	12.5	17.8	20.5
4 cm	1.2	1.1	1.1	1.0
5 cm	1.2	1.0	1.0	1.0
6 cm	1.1	1.0	1.0	1.0
7 cm	1.0	1.0	0.9	1.0
8 cm	1.0	1.0	1.0	1.0

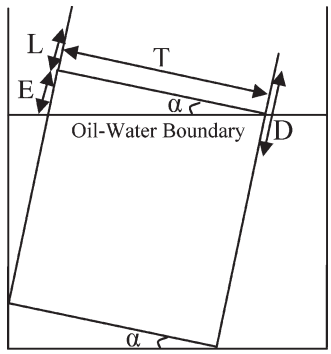

Fig. 11. Back-to-front tilting.

E. Wave Experiments

The experiments for both arrays were carried out using salt water at room temperature and under light conditions.

1) Light Sensor Array: The following is the analytical error analysis of the light sensor array, when it is moving back to front with the waves. In Fig. 11, D is the separation between two consecutive LDR centers strips, T is the distance between an LDR and a LED (in centimeters), and L is the difference between the oil–water boundary and the first LDR above it.

As shown in the geometry of Fig. 11, the worst case error in the thickness measurement for a back-to-front or front-to-back tilt is given by

$$\text{Error} = \text{ceiling}\left\{\frac{T \times \tan\alpha + L - \frac{D}{2}}{D}\right\} \times D. \qquad (3)$$

The error is divided by D, the ceiling is taken, and it is multiplied back by D to round it up to the nearest multiple of D, which is the resolution of the sensor. This rounding is needed since, in the worst case, the detection method results in an error in the measurement, as soon as the first LDR/LED below the oil–water boundary touches the oil (Fig. 11).

Moreover, the following is the error analysis when the array is tilting from right to left with the waves. As shown in the geometry of Fig. 12, which is perpendicular to the surface of

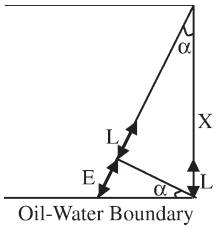

Fig. 12. Right-to-left tilting, where X is the thickness of oil.

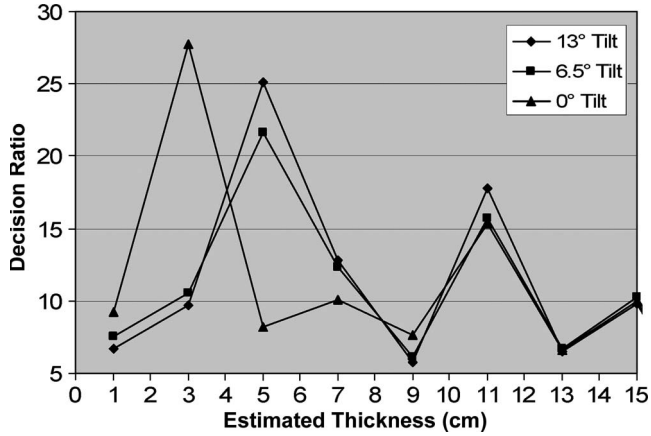

Fig. 13. Thickness measurement using LDRs (right-to-left tilt).

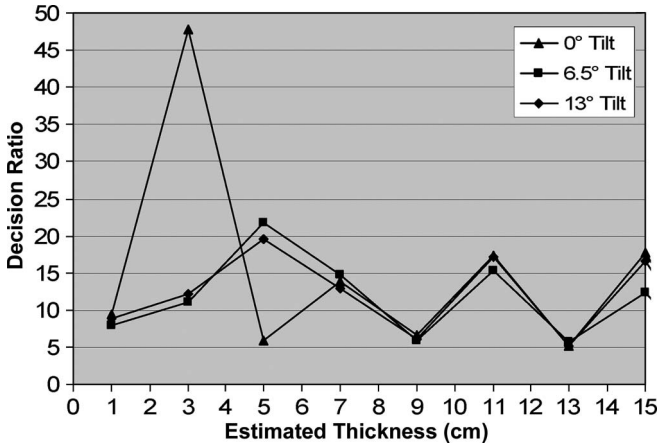

Fig. 14. Thickness measurement using LDRs (back-to-front tilt).

Fig. 11, the worst case error in the thickness measurement for a left-to-right or right-to-left tilt is given by

$$\text{Error} = \text{ceiling}\left\{\frac{X \times \tan\alpha \times \sin\alpha + L - \frac{D}{2}}{D}\right\} \times D. \quad (4)$$

Figs. 13 and 14 show the results of the simulated wave experiments, which were conducted with an oil thickness of 3 cm. In these experiments, the sensor was first tilted from back to front and then from right to left. Then, the measurements were taken at the tilted position. In both of these figures, whenever there is a tilt, the thickness is being incorrectly estimated by one resolution unit (2 cm). However, averaging several measurements and then applying the algorithm solve this problem. Thus, these experiments represent the worst case

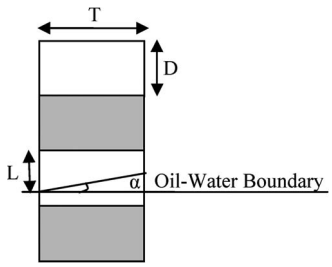

Fig. 15. Back-to-front tilting.

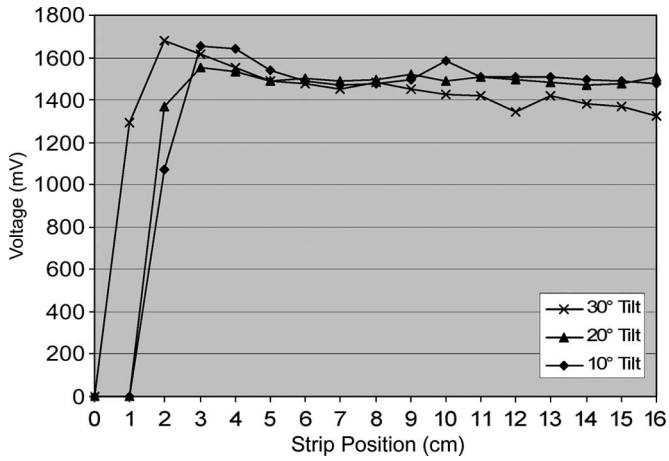

Fig. 16. Conductivity array results (right-to-left tilt).

scenario of the wavy situations, assuming that the sensor is not very stable.

2) Conductivity Array: The following is the analytical error analysis of the conductivity array, when it is moving back to front with the waves. In Fig. 15, the shaded strips represent the conductive strips, whereas the white strips represent the nonconductive strips. Here, D is the separation between two consecutive conducting strips, T is the width of each strip (in centimeters), S is the separation between the fully conductive plate and the stripped plate (in centimeters), and L is the difference between the oil–water boundary and the first conductive strip above it.

For a back-to-front tilt perpendicular to the surface of Fig. 15, the worst case error in the thickness measurement is given by

$$\text{Error} = \text{ceiling}\left\{\frac{S \times \tan\alpha - L + \frac{D}{2}}{D}\right\} \times D. \quad (5)$$

Moreover, as shown in the geometry of Fig. 15, the worst case error in the thickness measurement for a left-to-right or right-to-left tilt is given by

$$\text{Error} = \text{ceiling}\left\{\frac{T \times \tan\alpha - L}{D}\right\} \times D. \quad (6)$$

Figs. 16 and 17, along with Tables VI and VII, show the results of the simulated wave experiments. In these experiments, the sensor was first tilted from back to front and then from right to left. Then, the measurements were taken at the tilted position. In both of these figures, whenever there is a tilt, the thickness is being incorrectly estimated by one resolution unit

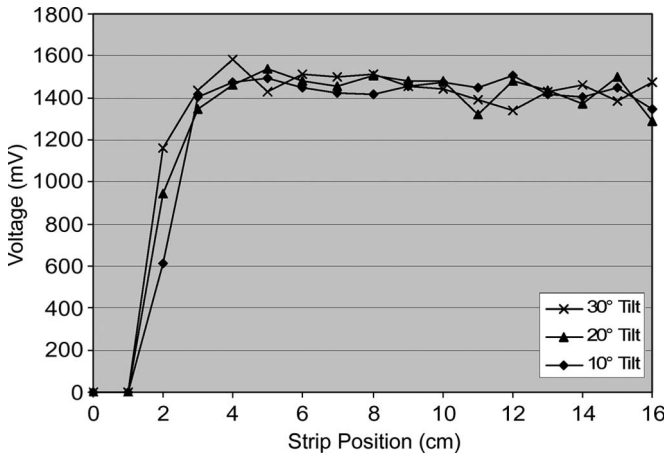

Fig. 17. Conductivity array results (back-to-front tilt).

TABLE VI
CONDUCTIVITY ALGORITHM RESULTS (RIGHT-TO-LEFT WAVES)

Estimated Thickness	Tilt Angle (Actual Thickness = 3 cm)		
	10°	20°	30°
1 cm	1.0	1.0	129133.3
2 cm	107133.3	137200.0	1.3
3 cm	1.5	1.1	1.0
4 cm	1.0	1.0	1.0

TABLE VII
CONDUCTIVITY ALGORITHM RESULTS (BACK-TO-FRONT WAVES)

Estimated Thickness	Tilt Angle (Actual Thickness = 3 cm)		
	10°	20°	30°
1 cm	1.0	1.0	3.0
2 cm	91850.0	94733.3	116266.7
3 cm	2.3	1.4	1.2
4 cm	1.1	1.1	1.1

(1 cm), except in one case, where the error is two units. As in the case of the light sensor array, this problem can be solved, and these experiments represent the worst case scenario of the wavy situation, compared with real-life scenarios where oil slicks, which are usually very heavy, limit the wave conditions in the sea. Moreover, cheap inclination sensors and accelerometers could be used to measure the wavy conditions and correct errors in the results of the device.

Furthermore, whenever none or all of the LDRs are covered with oil, the algorithm will compute a maximum ratio at some random thickness; thus, producing a wrong result. Unlike the conductivity array, this method is not suitable for the "no-oil" and "all-oil" cases. Moreover, the conductivity array has better resolution than the light sensor array, the resolution of which could be improved by reducing the distance between the centers of the LDRs (or using smaller LDRs). Although, for cleaning efforts, knowing the thickness up to 2-cm resolution (the light sensor array resolution) is acceptable, we note that the conductivity array can be designed to provide 1-mm resolution.

After assembling the whole device shown in Fig. 3, we tested its mechanical design in a large experimental tank with waves. The device was very buoyant and stable, and the top of the sensors was exactly at the air–water boundary, even with violent manually created waves. The maximum tilt of the device with the waves was almost 5°, which is much less than the worst case scenario previously accounted for. Moreover, it is worth noting that large oil spills typically form a thick shield over the water with significant surface tension, which inhibits the formation of waves.

TABLE VIII
POWER PROFILING

State of Operation	Power Consumption (mW)
Idle	833
LEDs - OFF	1725
LEDs - ON	2321
In-oil Conduct	1309
Light-array algorithm	1333
Conductivity algorithm	1273
Transceiver (TX)	10
GPS	220

F. Power Profiling

Since the sensor nodes are battery driven, energy profiling was necessary for the different components of the sensor for it to be operational during the lifetime of the spill cleanup. As the execution of the real code on the device and the realistic device timing is crucial for an accurate energy modeling of the sensor, then our energy profiling is based on direct measurements, which are performed using an oscilloscope, of the current drawn and the voltage supplied to each of the sensing boards, which include the microcontroller board, transceiver board, and GPS module board for their different states of operation (see Table VIII). The lifetime requirements of the sensor are easily satisfied using six 1.2-V batteries connected in series, each having a power rating of 3700 mAh.

VI. CONCLUSION

In this paper, a device that is capable of localizing and determining the oil thickness caused by an oil spill has been presented. The device utilizes two measurement methods that rely on the difference between the characteristics of oil and water. While the difference in blue light absorbance is detected using a light sensor array, the difference in electric conductivity is detected using a conductance array. The algorithms of these techniques have been presented and evaluated using extensive experiments. The mechanical design, hardware integration, and power profiling of the device have also been presented. The obtained results have been shown to be accurate and repeatable in the presence of different lighting, salinity, temperature, and wave conditions.

REFERENCES

[1] Greenpeace International, *Oil Spills—Philippines, Indian Ocean and Lebanon*, Aug. 18, 2006. greenpeace.org.
[2] M. F. Fingas and C. E. Brown, "Review of oil spill remote sensing," presented at the Int. Oil Spill Conf., Spillcon, Darwin, Australia, Aug. 16, 2000.
[3] F. Girard-Ardhuin, G. Mercier, and R. Garello, "Oil slick detection by SAR imagery: Potential and limitation," in *Proc. OCEANS*, 2003, pp. 164–169.
[4] G. Cai, J. Wu, Y. Xue, W. Wan, and X. Huang, "Oil spill detection from thermal anomaly using ASTER data in Yinggehai of Hainan, China," in *Proc. Geosci. Remote Sens. Symp.*, Jul. 23–28, 2007, pp. 898–900.

[5] J. Svejkovsky and J. Muskat, "Real-time detection of oil slick thickness patterns with a portable multispectral sensor," U.S. Dept. Interior Minerals Manage. Service, Herndon, VA, Jul. 31, 2006.
[6] O. N. Gershenzon, V. E. Gershenzon, and S. V. Osheyko, "Integral solution for oil spill detection using SAR data," in *Proc. 3rd Int. Conf. Recent Advances Space Technol.*, Jun. 14–16, 2007, pp. 361–365.
[7] T. Reddyhoff, S. Kasolang, R. Dwyer-Joyce, and B. Drinkwater, "The phase shift of an ultrasonic pulse at an oil layer and determination of film thickness," *J. Eng. Tribology*, vol. 219, no. 6, pp. 387–400, 2005.
[8] P. V. Panova, "The airborne remote systems for offshore oil seepage detection," in *Proc. Sci. Conf. 'SPACE, ECOLOGY, SAFETY' With Int. Participation*, Varna, Bulgaria, Jun. 10–13, 2005.
[9] C. E. Brown, "Airborne laser sensors for oil spill remote sensing," *Can. Chem. News*, vol. 49, no. 8, pp. 22–23, 1997.
[10] F. Salem, M. Kafatos, T. El-Ghazawi, R. Gomez, and R. Yang, "Hyperspectral image analysis for oil spill detection on contaminated land of urban areas," in *Proc. 3rd Int. Symp. Remote Sens. Urban Areas*, Istanbul, Turkey, Jun. 11–13, 2002.
[11] V. Byfield and S. R. Boxall, "Thickness estimates and classification of surface oil using passive sensing at visible and near-infrared wavelengths," in *Proc. Geosci. Remote Sens. Symp.*, 1999, pp. 1475–1477.
[12] Arjay Engineering Ltd. Technical Staff, *Model 2214-HCF Dual Channel Hydrocarbon Float Level Transmitter*, 2008, Oakville, ON, Canada: Arjay Eng. Ltd.
[13] S. A. Abdul-Wahab, "In situ device for detection of oil spill in seawater," *Electroanalysis*, vol. 18, no. 21, pp. 2148–2152, Sep. 2006.
[14] M. Chaplin, *Water Structure and Science*, Feb. 19, 2008. lsbu.ac.uk.
[15] O. Zbigniew, "Oil droplets as light absorbents in seawater," *Opt. Express*, vol. 15, no. 14, pp. 8592–8597, Jul. 2007.
[16] K. M. Almhdi, "Oil classification with fluorescence spectroscopy," M.E. thesis, Univ. Oldenburg, Oldenburg, Germany, 2005.
[17] V. Broje and A. A. Keller, "Interfacial interactions between hydrocarbon liquids and solid surfaces used in mechanical oil spill recovery," *J. Colloid Interface Sci.*, vol. 305, no. 2, pp. 286–292, Jan. 2007.
[18] A. Koulakezian, R. Ohannessian, H. Denkilkian, M. Chalfoun, M. K. Joujou, A. Chehab, and I. H. Elhajj, "Wireless sensor node for real-time thickness measurement and localization of oil spills," in *Proc. IEEE/ASME Int. Conf. AIM*, Xi'an, China, Jul. 2–5, 2008, pp. 631–636.

Hovig Denkilkian (S'08) is currently working toward the B.E. degree in computer and communication engineering from the Department of Electrical and Computer Engineering, American University of Beirut, Beirut, Lebanon.

He was a Research Assistant, working on medium-access control protocols for wireless sensor networks for more than a year. The outcome of the work was a paper "SN-MAC" published at the International Conference on Wireless Networks in 2008 (WORLDCOMP'08). His research interests include wireless communications, computer networks, wireless networks, and instrumentation.

Mr. Denkilkian was the recipient of the Creative Achievement Award from the Department of Electrical and Computer Engineering, American University of Beirut, for his work on his final year project in 2008.

Agop Koulakezian (S'07) was born in Beirut, Lebanon. He received the B.E. degree in computer and communications engineering (with high distinction) from the American University of Beirut (AUB), Beirut, in 2008. He is currently working toward the M.A.Sc. degree with the Department of Electrical and Computer Engineering, University of Toronto, Toronto, ON, Canada.

His research interests include instrumentation, wireless communications, and peer-to-peer networks.

Mr. Koulakezian was the recipient of numerous awards at the AUB, such as the Dean's Award for Creative Achievement and the Distinguished Graduate Award in recognition of high academic achievement and contribution to the Department.

Rostom Ohannessian (S'07) received the B.Eng. degree (with high distinction) in computer and communications engineering from the American University of Beirut (AUB), Beirut, Lebanon, in 2008. He is currently working toward the M.A.Sc. degree with the Department of Electrical and Computer Engineering, University of Toronto, Toronto, ON, Canada.

His research interests include sensor, relay, and computer networks.

Mr. Ohannessian was the recipient of the Creative Achievement Award from the AUB in June 2008.

Milad S. Chalfoun received the Civil and Environmental Engineering degree and the B.E. degree in electrical and computer engineering from the American University of Beirut, Beirut, Lebanon, in 2006 and 2008, respectively.

He is currently a Research and Development Engineer with Polytronics, Lebanon. His work encompasses the development of embedded systems, control for power stations, instrumentation, networking and custom database systems, human–machine interface, reverse engineering, and system penetration tests.

Mohamad Khaled W. Joujou received the B.E. degree in electrical engineering and the M.E. degree in mechanical engineering (mechatronics) from the American University of Beirut (AUB), Beirut, Lebanon, in 1997 and 2006, respectively.

He is currently a Laboratory Engineer/Manager with the Department of Electrical and Computer Engineering, AUB. His research interests include instrumentation, industrial control, and power electronics.

Mr. Joujou was the recipient of the Deans Award for outstanding creative achievement in July 1997.

Ali Chehab (SM'99) was born in Beirut, Lebanon. He received the B.E. degree in electrical engineering from the American University of Beirut (AUB), Beirut, in 1987, the Master's degree in electrical engineering from Syracuse University, Syracuse, NY, and the Ph.D. degree in electrical and computer engineering (ECE) from the University of North Carolina, Charlotte, in 2002.

From 1989 to 1998, he was a Lecturer with the Department of ECE, AUB. He rejoined the Department of ECE as an Assistant Professor in 2002 and became an Associate Professor in 2008. His research interests are very large scale integration testing, information security, and instrumentation.

Imad H. Elhajj (SM'97) received the B.E. degree (with distinction) in computer and communication engineering from the American University of Beirut (AUB), Beirut, Lebanon, in 1997 and the M.S. and Ph.D. degrees in electrical engineering from Michigan State University, East Lansing, in 1999 and 2002, respectively.

He is currently an Assistant Professor with the Department of Electrical and Computer Engineering, AUB. His research interests include instrumentation, sensor and computer networks, robotics, human machine interfacing, multimedia networking, and medical systems.